



## Article

# An archaeometric study of early Copper Age pottery from a cave in Romania

Alexandra Enea-Giurgiu<sup>1</sup> , Corina Ionescu<sup>1,2,3\*</sup> , Volker Hoeck<sup>1,3</sup>, Tudor Tămaş<sup>1</sup> and Cristian Roman<sup>4</sup>

<sup>1</sup>Department of Geology, Babeş-Bolyai University, 1 Kogălniceanu Str., 400084 Cluj-Napoca, Romania; <sup>2</sup>Institute of International Relations History and Oriental Studies, Archeotechnologies & Archeological Material Sciences Laboratory, Kazan (Volga Region) Federal University, 18 Kremlevskaya Str., 420000 Kazan, Tatarstan, Russia; <sup>3</sup>Division Geography and Geology, Paris Lodron University, 34 Hellbrunnerstraße, 5020 Salzburg, Austria and <sup>4</sup>Corvin Castle, 1–3 Castelului Str., 331141, Hunedoara, Romania

### Abstract

Early Copper Age pottery sherds discovered in a cave within the crystalline dolomites of the Southern Carpathians (Romania) were investigated by polarized light optical microscopy (OM), X-ray powder diffraction (XRPD) and electron microprobe analysis (EMPA) to obtain information on the pottery production in the Copper Age in the territory of present-day Romania. Microscopically, the clayey matrix of the ceramic body is highly birefringent or consists of low-birefringent and isotropic parts mixed together, containing fragments of quartz, muscovite, alkali feldspar, plagioclase, biotite, chlorite, heavy minerals and metamorphic and magmatic rocks, as well as an opaque material. The EMPA data revealed an Fe-rich illite-like matrix and helped to identify the mineral nature of the inclusions. Local pottery production in bonfires or surface clamps is envisaged. Miocene illitic clays may have been used as raw materials, mixed with a small amount of sandy temper. The thermal changes revealed by OM, the modification of the XRPD peaks and the EMPA data suggest firing temperatures of between 800 and 850°C.

**Keywords:** archaeometry, early Copper Age, EMPA, Foeni Group, pottery, Romania, XRPD

(Received 26 November 2018; revised 20 April 2019; Accepted Manuscript online: 25 July 2019; Associate Editor: Joao Labrincha)

Ceramic remnants potentially bear significant information about ancient societies, in particular prehistoric ones. In some cases, a few sherds may indicate the technological level and knowledge of the environment, including sources of raw materials. When characterizing ceramic artefacts recovered from archaeological sites, complex scientific approaches are commonly used because a mere macroscopic investigation may not offer answers to questions regarding the raw materials, the modelling or the firing conditions. Findings from caves are particularly important as they may reflect either a permanent settlement or a temporary use of the area. The latter might have been related to various activities such as hunting, plant gathering and forest exploitation. Caves were also provisory refuges in times of danger.

The beginning of the Copper Age in Banat (the southwestern part of present-day Romania) and Transylvania (the central part of present-day Romania) is marked by the onset of the so-called ‘Foeni Group’ culture and shows distinct social and economic features (Gligor, 2014). More than 20 archaeological sites have been assigned to this group (Gligor, 2008a). The only Foeni-type sherds investigated archaeometrically so far have been those excavated at the Lumea Nouă–Alba Iulia site in southwest Transylvania (Fabbri *et al.*, 2008, 2009; Bințișan *et al.*, 2019) and in some sites in Banat (Spataro, 2011).

The aim of this study was to obtain information on pottery production at the dawn of the Copper Age in the Southern Carpathians

(Romania), an area subject to multiple cultural influences. Taking into account the general scarcity of Foeni ceramic artefacts, even a small number of sherds may offer essential social, economic and technological information. Pottery sherds excavated in the Great Cave of Cerișor (GCC) from the Southern Carpathians were studied mineralogically and petrographically using polarized light optical microscopy (OM), X-ray powder diffraction (XRPD) and electron microprobe analysis (EMPA). The OM provides information on the optical character of the matrix and the mineralogy/petrography of the clasts (Maggetti, 1979, 1982), whereas the XRPD helps to determine mineral species and thermal changes (Heimann, 2017). Electron microprobe analysis is a basic tool for determining the exact chemistry of phases and thus precisely identifying the minerals (Ionescu *et al.*, 2011; Ionescu & Hoeck, 2017). We aimed to define compositionally the sherds and to assess the technological conditions of pottery production. The results obtained were compared with previous published data on pottery found in the same cave in order to identify the raw materials potentially involved in obtaining the ceramic paste.

### Archaeological context

The caves from the Poiana Ruscă Mountains in the Southern Carpathians contain various remnants of Neolithic cultures. The most famous among these caves are the Cauce Cave (Spataro, 2011; Drașovean, 2013) and the GCC (*Peștera Mare de la Cerișor* in Romanian) (Fig. 1). The latter opens on the right slope of the Runc Valley at ~2.5 km northeast of Cerișor village (coordinates: N45°45′7.74″ and E22°46′18.54″). At the entry, there is a large room 20 m × 5 m × 6 m in size, with a floor

\*E-mail: [corina.ionescu@ubbcluj.ro](mailto:corina.ionescu@ubbcluj.ro)

Cite this article: Enea-Giurgiu A, Ionescu C, Hoeck V, Tămaş T, Roman C (2019). An archaeometric study of early Copper Age pottery from a cave in Romania. *Clay Minerals* 54, 255–268. <https://doi.org/10.1180/clm.2019.35>

**Fig. 1.** Location of the GCC (Peștera Mare de la Cerișor) on a simplified geological map (based on Gherasi *et al.*, 1967; Mureșan *et al.*, 1980). The upper-right insert shows the position of the map within Romania. The image is modified from Giurgiu *et al.* (2017). The map also shows the area of Miocene clays sampled by Giurgiu *et al.* (2017) and the presumed location of pottery production in the Copper Age.

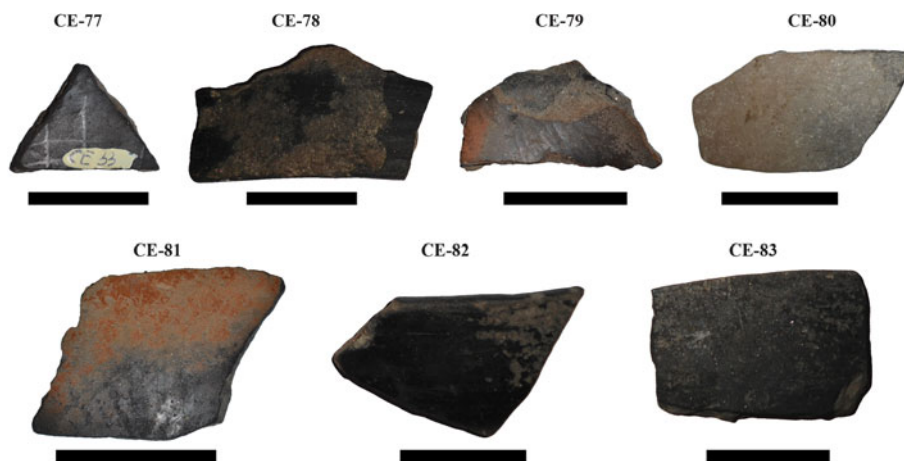
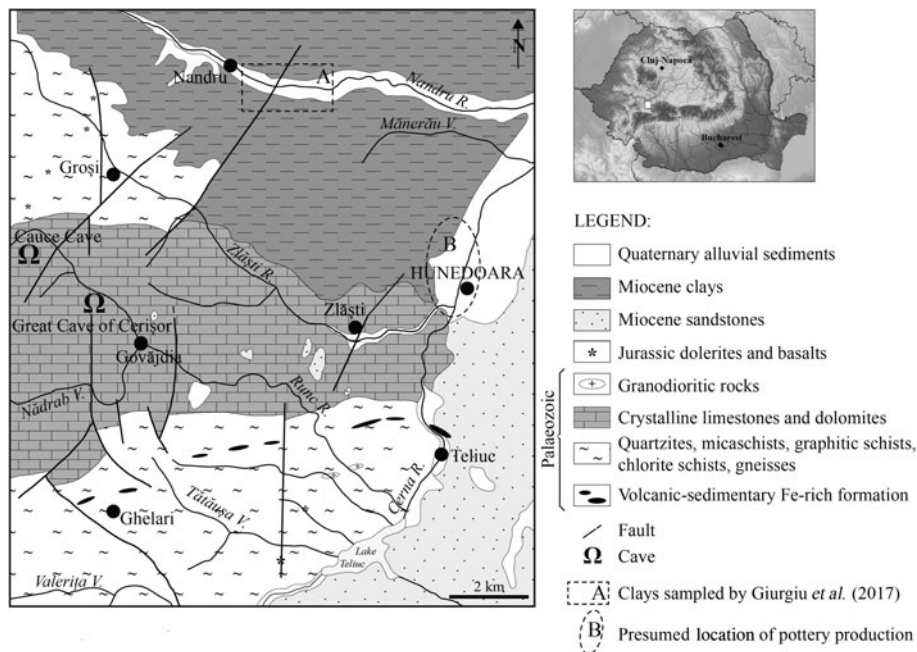


**Fig. 2.** Foeni Group potsherds from the GCC, consisting of patterned (CE-77) and plain burnished samples (CE-78, CE-79, CE-81, CE-82 and CE-83). Scale bars = 3 cm.

covered in a layer of clay and silty clay mixed with dolomite fragments. The discovery of ceramic sherds in these cave sediments triggered subsequent archaeological investigation. From the two pits excavated in 2000, potsherds, copper adornments and lithic tools have been unearthed (Roman *et al.*, 2000). The archaeological finds from the cave were assigned to several cultures (*i.e.* the late Neolithic Turdaș, the early Copper Age Foeni, the Copper Age Coțofeni and the Bronze Age Wietenberg), indicating a human presence from the late Neolithic to the Bronze Age. So far, only the pottery sherds attributed to the Copper Age Coțofeni culture have been studied (Giurgiu *et al.*, 2017).

The Foeni Group culture was dated by a radiocarbon technique to a timespan between 4750 and 4400 BCE (*i.e.* at the beginning of the Copper Age) (Drașovean, 2013; Gligor, 2014). In today's Romanian territory, the first signs of this culture occurred in the southwest, in the Banat region, and later spread towards the northeast, into an area known as Transylvania. This culture is regarded as a precursor to the well-known Cucuteni and Petrești Copper Age cultures (Drașovean, 2013; Gligor, 2014). Foeni pottery is predominantly fine and semifine, rarely coarse (Gligor, 2007a) and consists of bowls, porringers,

amphorae, cups and platters (Luca *et al.*, 2004; Gligor, 2007a, 2008b, 2009a). It is typically red and black-topped (Gligor, 2009b, 2014; Bințișan & Gligor, 2016) and has plain and pattern burnished surfaces (Drașovean, 1994; Gligor, 2007b; Fabbri *et al.*, 2009). Decorations include grooves, incisions, imprints, painted strips, beads and circular and conical knobs (Gligor, 2007a, 2009a).

So far, no remains from pits, surface clamps or kilns from the surroundings of the GCC or from the areas towards the north and east (Fig. 1), where potential clayey raw materials occur, have been documented. There are several reasons for this, including the fragile nature of such constructions, the intense modern agricultural work in the area and the difficulty of distinguishing the remains of firing structures from other archaeological structures (Thér, 2004).

### Geological background

The GCC is located in the Palaeozoic crystalline dolomites of the Southern Carpathians (Gherasi *et al.*, 1967; Mureșan *et al.*, 1980; Balintoni, 1997; Balintoni *et al.*, 2009, 2014). Other metamorphic rocks, such as micaschists, quartzites, gneisses, graphitic schists,

**Table 1.** Macroscopic characteristics of the Foeni potsherds.

Sample no.	Sherd surface			Ceramic wall structure and colour (Munsell, 1994)		
	Slip	Colour (of the rim/slip)	Burnish	Type	Core	Rim(s)
CE-77	Inside and outside	GLE Y1 4/N dark grey	Pattern, outside	Homogeneous	2.5 YR 5/4 reddish-brown	–
CE-78	Inside and outside	GLE Y1 4/N dark grey	Plain, inside and outside	Homogeneous	2.5 YR 5/4 reddish-brown	–
CE-79	Inside	2.5 YR 4/3 reddish brown	Plain, inside and outside	Sandwich	GLE Y1 3/N very dark grey	2.5 YR 6/4 light reddish brown
CE-80	Missing	7.5 YR 7/1 grey	Plain, inside	Bizonal	GLE Y1 4/N dark grey	7.5 YR 7/1 grey
CE-81	Missing	GLE Y1 4/N dark grey + 2.5 YR 5/8 red	Plain, outside	Homogeneous	GLE Y1 4/N dark grey	–
CE-82	Inside and outside	GLE Y1 4/N dark grey	Plain, inside and outside	Homogeneous	2.5 YR 5/4 reddish-brown	–
CE-83	Inside and outside	GLE Y1 4/N dark grey	Plain, inside and outside	Homogeneous	2.5 YR 5/4 reddish-brown	–

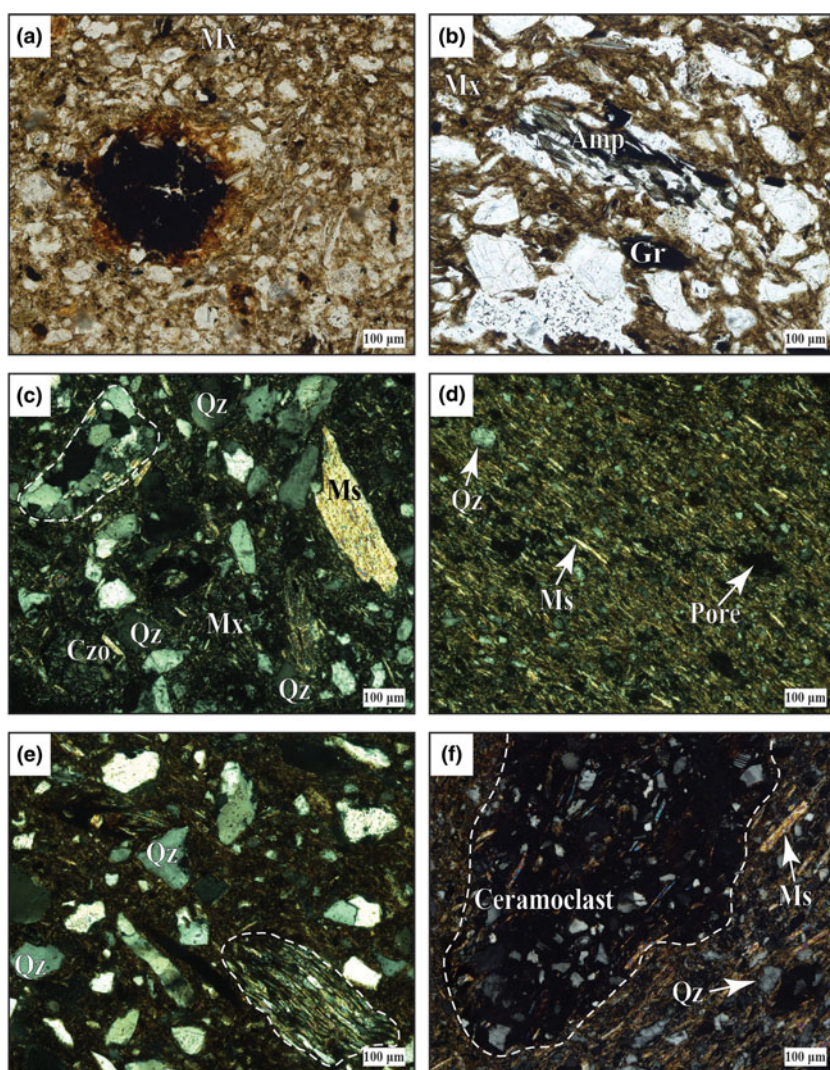


**Fig. 3.** Polarized light micrographs of the Foeni potsherds. (a) Iron pellet (black) showing a light diffusion aureole merging into the surrounding, translucent matrix (Mx) in sample CE-86. (b) Fragment of amphibolite schist (Amp) and a lamella of graphite (Gr) in sample CE-79. (c) Quartzo-feldspathic lithoclast marked with a dashed line, quartz (Qz), muscovite (Ms) and clinozoisite (Czo) in a birefringent matrix in sample CE-79. (d) Oriented texture in sample CE-81. (e) Quartz and micaschist (marked by a dashed line) fragments in sample CE-79. (f) Large ceramoclast (marked by a dashed line) in sample CE-83. Mineral abbreviations are according to Whitney and Evans (2010) and are used throughout this paper. Images (a) and (b) were obtained with one polarizer, and all others with crossed polarizers.

amphibolitic schists and crystalline limestones, crop out in the area (Fig. 1). Metamorphosed volcanic–sedimentary formations containing Fe ore (Kräutner, 1977) occur mostly in the south and southeast. West of the town of Teliuc (Fig. 1), there are small bodies of Jurassic dolerites and basalts. Palaeozoic granodiorites have been mapped south of Zlăști village. The area towards the northeast and north is covered by the Miocene

sediments of the Transylvanian Basin. The Miocene mudstone areas are currently used for various household purposes, including pottery. The riverbeds are filled with Quaternary sands and gravels. The main river in the area, Cerna, transports quartz, feldspar, muscovite, biotite and chlorite, various heavy minerals and fragments of rocks from its large catchment within the Southern Carpathians.

**Table 2.** Phase composition of the ceramic sherds as determined by optical microscopy.

Sample no.	Matrix (P+)	Non-plastic inclusions					
		Crystalclasts	Lithoclasts	Pedogenic concretions	Iron pellets	Clay pellets	Ceramoclasts
CE-77	Mixed (birefringent + isotropic)	Qz, Ms, Bt, Pl, Ep, Czo	Quartzite	+	+	+	-
CE-78	Birefringent	Qz, Ms, Bt, Pl, Czo	-	+	+	-	-
CE-79	Mixed (birefringent + isotropic)	Qz, Ms, Bt, Pl, Afs, Ap, Ep, Czo, St, Grt, Gr	Qz-Fsp rock, micaschist, amphibolite schist	+	+	+	-
CE-80	Birefringent	Qz, Ms, Bt, Chl, Ep, Czo, Grt	Qz-Fsp rock, micaschist	-	+	-	-
CE-81	Birefringent	Qz, Ms, Bt, Pl	-	+	+	-	-
CE-82	Birefringent	Qz, Ms, Bt, Pl, Ep	-	+	+	-	+
CE-83	Birefringent	Qz, Ms, Bt, Pl, Afs, Ep, Czo	Chlorite schist	+	+	+	+

Plus signs indicate presence; minus signs indicate absence.

Afs = alkali feldspar; Ep = epidote; Grt = garnet; P+ = crossed polarizers; Pl = plagioclase; St = staurolite.

## Samples and analytical methods

The seven sherds found in the cave that could be assigned to the Foeni Group with certainty (Fig. 2, Table 1) were too small to infer vessel typology. The sherds have a shiny appearance due to burnishing, either on the outer surface or on both outer and inner surfaces (Giurgiu *et al.*, 2015). All samples, except sherd sample CE-77, which is decorated by a 'pattern burnish', show so-called 'plain burnishing' covering the entire surface (see Ionescu *et al.*, 2015). The 'pattern burnish' (sherd CE-77) consists of a grid of ~1 mm-wide shiny lines on a smoothed, matte surface. A similar decoration was described for potsherds assigned to the same cultural group (Foeni) and found in the southwestern part of Transylvania (Roman *et al.*, 2000). The GCC potsherds have a dark grey to reddish-brown surface. Three samples (CE-79, CE-80 and CE-81) display a gradual transition between the reddish and the dark grey areas and are most probably parts of black-topped pots. Small (<1 mm) muscovite lamellae are visible on the surface of samples CE-79, CE-80 and CE-82. Some of the potsherds display a dark grey slip (*e.g.* CE-77 and CE-82) and one sample has a reddish-brown slip (CE-79). The thickness of the ceramic wall varies between 5 and 11 mm. The sherds show a homogeneous reddish-brown (CE-77, CE-78, CE-82 and CE-83) or grey (CE-81) ceramic wall. One sample (CE-80) displays a bizonal structure, half dark grey and half grey. The so-called 'sandwich' structure was identified in sample CE-79, with up to 1 mm-thick outer rims.

The mineralogical composition and the fabric (texture and structure) of the sherds as well as the optical character of the matrix were studied by polarized light OM. Slices a few millimetres thick were cut across the ceramic wall with a diamond saw in order to prepare thin sections for OM and polished thin sections for EMPA. After cutting, the slices were cleaned with distilled water. OM was carried out at the Department of Geology (Babeş-Bolyai University Cluj-Napoca) with an Axio Imager.A2m Zeiss transmitted light-polarizing microscope equipped with a Zen 2011 Axio high-resolution digital video camera.

In order to determine the crystalline mineral phases, a few grams from each potsherd were hand-milled in an agate mortar and analysed by XRPD with a Bruker D8 Advance diffractometer with a Bragg-Brentano geometry (Department of Geology, Babeş-Bolyai University in Cluj-Napoca) at 35 kV and 45 mA using Co-K $\alpha_1$  radiation ( $\lambda = 1.78897$ ), an Fe 0.01 mm filter and

a one-dimensional detector. The data were collected between 5° and 64°2 $\theta$  using a 0.02°2 $\theta$  step and a 0.2 s counting time per step. The SRM 1976a corundum (US National Institute of Standards and Technology reference material; [www.nist.gov/programs-projects/powder-diffraction-srms](http://www.nist.gov/programs-projects/powder-diffraction-srms)) was used for calibration purposes. For mineral identification, the XRPD data were compared with Bruker's *Diffrac.Eva 2.1* software, data from the International Center for Diffraction ([www.icdd.com](http://www.icdd.com)) and data from Caroll (1970) and Moore & Reynolds (1997).

Two polished thin sections (CE-80 and CE-83), coated with carbon under vacuum, were analysed at Salzburg University with a JXA Superprobe 8600 electron microprobe, equipped with four wavelength-dispersive spectrometers and one Si(Li) energy-dispersive spectrometer to determine the microchemistry of the phases comprising the matrix in particular clay minerals and muscovite. Heavy minerals and Fe-rich materials were also identified by EMPA. The equipment operated at a 15 kV accelerating voltage, a 40 nA beam current and a  $\leq 3$   $\mu\text{m}$  electron-beam diameter. For back-scattered electron (BSE) image acquisition, the beam current was reduced to 10–15 nA. The description of the analytical details follows Ionescu & Hoeck (2011). The following standards were used: quartz (for SiO<sub>2</sub>), synthetic  $\gamma$ -alumina (for Al<sub>2</sub>O<sub>3</sub>), synthetic iron oxide (for FeO<sub>TOT</sub>), rutile (for TiO<sub>2</sub>), apatite (for CaO and P<sub>2</sub>O<sub>5</sub>), synthetic periclase (for MgO), halite (for Na<sub>2</sub>O), sylvite (for K<sub>2</sub>O), pyrolusite (for MnO) and barium glass (for BaO). The final chemical composition was calculated following the atomic number effect correction (known as 'ZAF'), based on the relation between concentration and X-ray intensity (Heinrich, 1991). The detection limits were 0.02 mass% for MgO, CaO, Na<sub>2</sub>O and K<sub>2</sub>O, 0.03 mass% for Al<sub>2</sub>O<sub>3</sub> and MnO, 0.04 mass% for TiO<sub>2</sub>, 0.05 mass% for SiO<sub>2</sub>, 0.06 mass% for FeO and 0.07 mass% for P<sub>2</sub>O<sub>5</sub> and BaO. The counting times were 20 s for each peak and 10 s for the background. The analytical data are presented in mass%, according to the International System of Units (Taylor, 2001).

## Results

### Optical microscopy

The potsherd bodies consist of two major components: (1) a matrix (*i.e.* a mixture of thermally transformed clay minerals and aplastic (micro)clasts); and (2) various aplastic (macro)clasts – referred to here as 'clasts' (Fig. 3a–f). The border between these

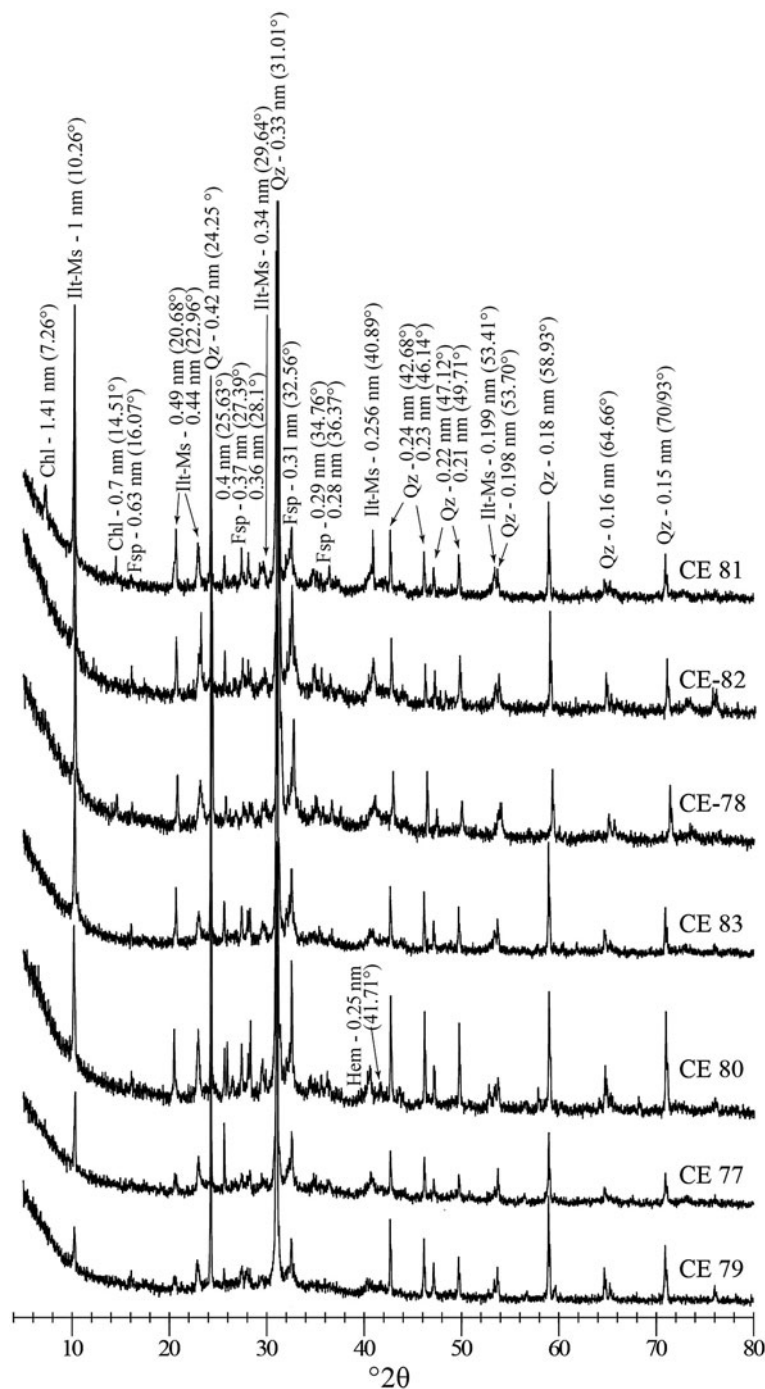


Fig. 4. XRD traces of the Foeni sherds. Fsp = feldspar; Hem = hematite; Illt-Ms = illite-muscovite; Chl = chlorite; Qz = quartz.

components is conventionally set at either 0.015 mm (Maggetti, 1979) or 0.02 mm (Ionescu *et al.*, 2011). The texture is not oriented (Fig. 3b,c,e) and has a random arrangement of phyllosilicate lamellae (Fig. 3b,c). Samples CE-80 and CE-81 locally show an oriented texture (Fig. 3d,f).

Under plane-polarized light, the matrix is translucent and light to dark brown in colour (Fig. 3a,b) and sometimes contains a fine-grained opaque phase. With crossed polarizers, the matrix is highly birefringent in most samples (Fig. 3c,d,f) and shows only thin isotropic areas between the clay minerals, due to sintering. Only samples CE-77 and CE-79 show a lower birefringence and larger but isolated isotropic areas (Fig. 3e). The clay minerals

are prevalent in the matrix but cannot be identified due to the limitations of OM resolution. Microclasts of quartz (Fig. 3c–f), muscovite, biotite, plagioclase, alkali feldspar, apatite, epidote, clinozoisite and unidentified opaque minerals were identified as components of the matrix (Table 2).

The macroclasts (>0.02 mm in size) are mostly quartz, micas, plagioclase and alkali feldspar, besides various lithoclasts, opaque phases and heavy minerals. Quartz is angular or subangular and displays a network of cracks in some cases. Muscovite occurs as large (Fig. 3c) or small (Fig. 3d,f) lamellae. Biotite is either fresh or partly altered to chlorite accompanied by opaque minerals. Lamellae of discrete chlorite are also present. Polysynthetically

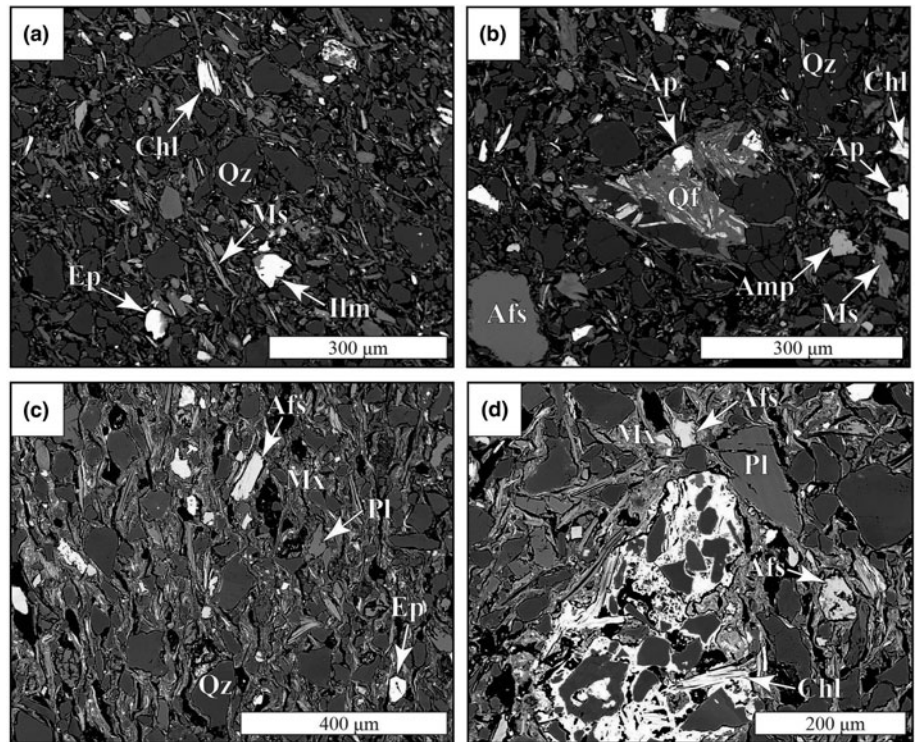


**Fig. 5.** BSE images of the ceramic body. (a) Inhomogeneous appearance of sample CE-80, with quartz (Qz), muscovite (Ms), epidote (Ep), chlorite (Chl) and ilmenite (Ilm) grains in a highly porous, illite-like matrix. (b) Fragments of quartz, alkali feldspar (Afs), muscovite, apatite (Ap), amphibole (Amp), and a quartzo-feldspathic rock (Qf) in sample CE-80. (c) Quartz, alkali feldspar and plagioclase crystalloclasts (Pl) in sample CE-83. (d) Fragment of chlorite schist in sample CE-83. The black areas in all images are pores.

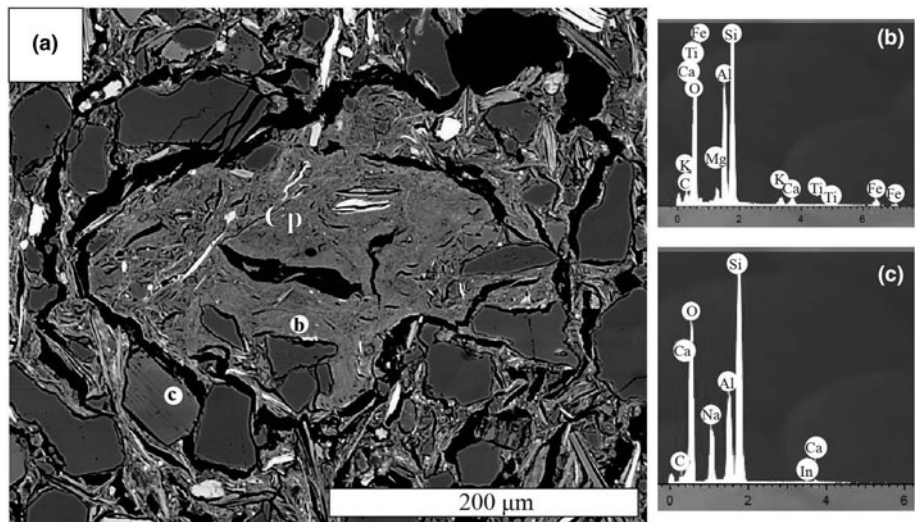


**Fig. 6.** (a) BSE image of a clay pellet (Cp) rimmed by a contraction void in sample CE-83. (b) Energy-dispersive spectra of the clay mineral forming the pellet. (c) Energy-dispersive spectra of a plagioclase grain. The white dots in (a) marked with (b) and (c) show the locations where the energy-dispersive spectra were collected.

twinned plagioclase is frequent. The grains of alkali feldspar are slightly altered to fine-grained muscovite ('sericite'). Heavy minerals are diverse: epidote, clinozoisite, staurolite, amphibole, garnet and apatite. The lithoclasts are scarce and include quartzite, micaschist (Fig. 3e), amphibolitic schist (Fig. 3b) and quartzo-feldspathic rock (Fig. 3c).

Opaque material 25–50 μm in size is ubiquitous and is distributed unevenly in the ceramic body (Fig. 3a). It probably consists of iron pellets ('bohnerz'; Maggetti, 1979), Fe-rich pedogenic concretions and graphite lamellae (Fig. 3b). Clay pellets have also been identified. The ceramoclasts (*i.e.* fragments of chamotte) are restricted to sherds CE-82 and CE-83 (Table 2, Fig. 3f).

Granulometrically, two groups of clasts were identified, marking a so-called 'hiatal' structure. The first group includes grains <0.02 mm in size, within the range of the matrix. The second

group includes most of the clasts, up to 0.6 mm in size, with an average of between 50 and 100 μm. The clasts from the latter group are classified within the coarse silt and the very fine sand (Wentworth, 1922). Granulometrically, only sample CE-79 is semifine; the remaining samples are fine-grained.

#### X-ray powder diffraction

The XRPD traces show a fairly uniform mineralogical composition for the sherds, with quartz, an illite-like phase, muscovite and feldspars as the main mineral phases (Fig. 4). The 1 nm, 0.45 nm and 0.26 nm peaks are common to both an illite-like mineral and muscovite, so the term 'illite-muscovite' will be used hereafter. The XRPD traces are arranged according to the appearance of the 1 nm illite-muscovite peak (Fig. 4), from the

**Table 3.** Selected EMPAs (mass%) and calculated structural formulae for the illite-like matrix in the Foeni ceramics.

Sample/micropoint	CE-80-2-13	CE-80-2-14	CE-80-2-6	CE-80-3-15	CE-80-3-16	CE-80-3-3	CE-80-3-4	CE-83-1-4	CE-83-1-8	CE-83-3-1	CE-83-3-13	CE-83-3-2	CE-83-3-4	CE-83-3-7
SiO <sub>2</sub>	47.62	51.45	48.03	48.54	47.01	46.51	58.41	45.3	45.34	43.65	45.25	43.3	44.28	45.94
Al <sub>2</sub> O <sub>3</sub>	29.30	27.17	27.54	19.12	24.63	23.60	18.59	22.18	23.86	22.57	22.41	22.02	22.39	22.37
TiO <sub>2</sub>	0.17	0.76	1.22	0.33	0.62	0.46	0.18	0.74	0.61	0.54	0.81	0.69	0.82	0.63
FeO	2.15	5.10	5.03	5.50	6.73	9.39	3.02	6.06	6.81	7.03	8.46	7.86	7.75	6.89
MnO	bdl	0.03	0.08	0.05	bdl	0.07	0.05	bdl	bdl	bdl	0.03	bdl	0.03	0.03
MgO	1.69	2.32	2.25	2.91	2.35	4.48	1.31	2.35	2.13	2.15	2.8	2.21	2.17	2.59
CaO	1.39	1.10	1.38	1.86	1.25	1.20	0.88	1.62	2.68	2.46	2.67	2.52	2.41	2.79
Na <sub>2</sub> O	0.17	0.32	0.40	0.31	0.41	0.36	1.38	0.26	0.32	0.17	0.23	0.18	0.21	0.26
K <sub>2</sub> O	7.87	6.47	5.54	3.48	4.76	3.98	3.52	3.32	3.31	1.78	2.01	1.69	1.67	2.09
P <sub>2</sub> O <sub>5</sub>	0.33	0.13	0.08	bdl	bdl	bdl	bdl	0.24	1.68	0.66	2.37	1.15	0.25	2.77
Total	90.23	94.65	91.45	81.98	87.63	89.90	87.26	81.76	84.96	80.33	84.54	80.44	81.69	83.43
Si	6.59	6.83	6.61	7.36	6.78	6.63	8.08	6.91	6.58	6.74	6.55	6.67	6.79	6.62
Al <sup>IV</sup>	1.41	1.17	1.39	0.64	1.22	1.37	0	1.09	1.42	1.26	1.46	1.33	1.21	1.38
Sum T	8	8	8	8	8	8	8.08	8	8	8	8	8	8	8
Al <sup>VI</sup>	3.36	3.07	3.08	2.78	2.96	2.59	3.03	2.89	2.66	2.84	2.36	2.66	2.83	2.42
Ti	0.02	0.08	0.13	0.04	0.07	0.05	0.02	0.09	0.07	0.06	0.09	0.08	0.10	0.07
Fe <sup>2+</sup>	0.25	0.57	0.58	0.70	0.81	1.12	0.35	0.77	0.83	0.91	1.02	1.01	0.99	0.83
Mn	0	0	0.01	0.01	0	0.01	0.01	0	0	0	0	0	0	0
Mg	0.35	0.46	0.46	0.66	0.51	0.95	0.27	0.53	0.46	0.50	0.60	0.51	0.50	0.56
Ca	0.21	0.16	0.20	0.30	0.19	0.18	0.13	0.27	0.42	0.41	0.41	0.42	0.40	0.43
Na	0.05	0.08	0.11	0.09	0.12	0.10	0.37	0.08	0.09	0.051	0.07	0.05	0.06	0.07
K	1.39	1.10	0.97	0.67	0.88	0.720	0.62	0.65	0.61	0.35	0.37	0.33	0.33	0.38
P	0.04	0.01	0.01	0.01	0.01	0	0	0.03	0.21	0.09	0.29	0.15	0.03	0.34
Total cations	13.62	13.51	13.54	13.25	13.53	13.73	12.87	13.28	13.14	13.12	12.93	13.06	13.20	12.77
Fe/(Fe + Mg)	0.42	0.55	0.56	0.51	0.62	0.54	0.56	0.59	0.64	0.65	0.63	0.67	0.67	0.6

Fe<sub>TOT</sub> as FeO.Calculations on a 22 O basis, according to Deer *et al.* (1992).

bdl = below detection limit; Sum T = total cations in tetrahedral sites.

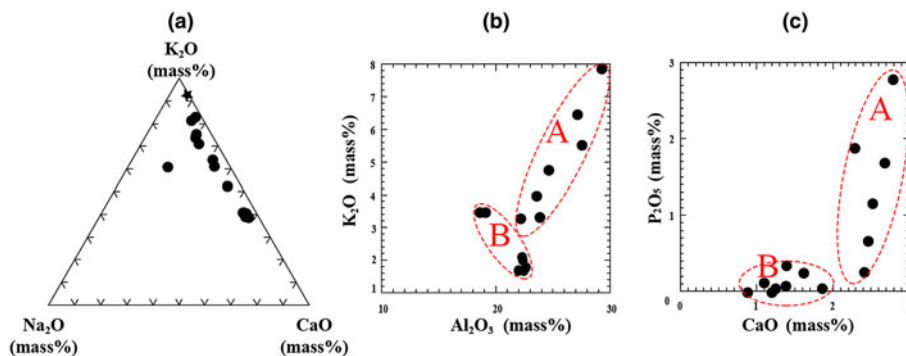


**Fig. 7.** Plot of the EMPA data obtained for the matrix in the (a)  $K_2O$ - $Na_2O$ - $CaO$ , (b)  $Al_2O_3$  vs.  $K_2O$  and (c)  $CaO$  vs.  $P_2O_5$  discrimination diagrams. Black star = illite; black dots = Foeni samples. The dashed lines demark the groups.

most intense (at the top of Fig. 4) to the least intense (at the bottom of Fig. 4). The sharp, narrow and intense 1 nm peak of the sherds with a highly birefringent matrix (e.g. samples CE-81 and CE-82) demonstrates a crystalline structure. The CE-77 and CE-79 sherds, containing a low-birefringent matrix mixed with isotropic material, show a slightly diminished 1 nm peak due to the partial destruction of the crystalline structure during firing.

The feldspar peaks are more intense for the sherds with intense illite-muscovite peaks. The wide diffraction peak at 1.4 nm may be assigned to both chlorite and montmorillonite. Weak hematite peaks (0.25 and 0.27 nm) occur in all samples.

#### Electron microprobe analysis

The BSE images and the energy-dispersive spectra (Figs 5a-d, 6a-c) reveal a porous ceramic body that is chemically and mineralogically inhomogeneous at a small scale. The matrix consists of a very fine-grained mixture of clay mineral and muscovite, as well as quartz, feldspars and heavy minerals. The individual clay mineral and sometimes muscovite lamellae are difficult to separate visually due to a smooth transition caused by sintering (Figs 5a-d, 6a). The microchemistry of the clay mineral and muscovite forming the matrix of the Foeni sherds (Table 3) is comparable with data obtained for the Copper Age Coțofeni pottery found in the same cave (Giurgiu *et al.*, 2017). The clay mineral is illite-like and can be distinguished from muscovite (Fig. 5b) by a darker greyish hue and a greater amount of  $SiO_2$ . Overall, in the clayey part of the matrix including muscovite,  $SiO_2$  ranges from ~43 to >58 mass% and  $Al_2O_3$  from ~18 to ~30 mass%. The  $K_2O$  content also varies widely, from 1 to almost 8 mass%.

In the  $K_2O$ - $Na_2O$ - $CaO$  ternary diagram (Fig. 7a), our matrix data plot is different from that of illite (Deer *et al.*, 1992), towards increasing  $CaO$ . The high  $Al_2O_3$  content suggests a slightly altered muscovite. On a positive correlation background between  $Al_2O_3$  and  $K_2O$ , two groups are separated (Fig. 7b), one related to an illite-dominated matrix (A) and another reflecting a muscovite-dominated matrix (B).

The  $FeO_{TOT}$  content in the matrix is also highly variable, between 2 and >9 mass%, whereas the amount of  $CaO$  and  $P_2O_5$  is <3 mass%. The diagram in Fig. 7c shows two groups of data. The first group includes a matrix with high calcium and increasing phosphorous contents and reveals a slightly positive correlation between these elements. The second group has low phosphorous and low calcium contents and shows no correlation.

The quartz clasts in the ceramic body are almost pure, with 99.14 mass%  $SiO_2$ . The alkali feldspar (Table 4, Figs 5b,c, 8) is predominantly orthoclase, with <10% albite. The albite content

in the plagioclase (Fig. 5c) ranges between  $Ab_{92}$  (albite) and  $Ab_{67.9}$  (andesine), with a prevalence of oligoclase. The plagioclase does not display compositional zoning.

Chlorite (Fig. 5a,b,d), muscovite (Table 5) and heavy minerals such as clinozoisite, epidote, ilmenite (Fig. 5a), apatite and amphibole (Fig. 5b), were determined by EMPA. Chlorite schist fragments, iron pellets/pedogenic concretions and clay pellets (Fig. 6a) were also measured microchemically.

The iron pellets/pedogenic concretions contain up to 20 mass%  $Fe_2O_3$ , ~13 mass%  $Al_2O_3$ , ~4.5 mass%  $P_2O_5$ , ~4.2 mass%  $CaO$ , ~35 mass%  $SiO_2$  and ~10 mass%  $TiO_2$ . With  $FeO_{TOT}$  up to 5 mass% and  $MgO$  up to 3.5 mass%, muscovite shows a phengitic character.

The X-ray compositional mapping (Fig. 9) shows the distribution of Si, Al, K, Ca and Fe in the ceramic sherds. The density of the tiny dots reflects the relative element concentrations in the mineral phases (Ionescu & Hoeck, 2017). Si is related to quartz and various silicates (illite-mineral, feldspars and muscovite). Al is the main component of aluminosilicates (illite-mineral, feldspars and muscovite), whereas K reflects minerals such as alkali feldspars and clay minerals (matrix). Calcium and iron are very finely dispersed within the matrix consisting of clay minerals and are not linked to specific phases.

## Discussion

### Inferring raw materials

The information on possible raw clayey materials used to produce Foeni pottery was derived from XRPD and EMPA data, whereas OM provides hints as to the temper that was used. The mineral nature and microchemistry of the clay minerals and heavy minerals are especially important, as they reflect the geological background of the area.

The XRPD traces show that the ceramic mass consists mainly of an illite-like mineral, muscovite and quartz in all Foeni sherds (Fig. 4). The EMPA microchemistry of the matrix (Table 3, Fig. 7a,b) also shows an illite-like material, but it is slightly depleted in  $K_2O$  and slightly enriched in  $CaO$  compared to illite (Deer *et al.*, 1992). A similar chemical composition with a tendency to incorporate calcium into the illite-like structure was described in the Copper Age ceramic matrix by Ionescu & Hoeck (2011). The  $CaO$  is probably due to a small amount of montmorillonite in the raw clay (see also Gál *et al.*, 2018). However, with <3 mass%  $CaO$ , the matrix points to a poorly carbonatic clay.



**Table 4.** Selected EMPAs (mass%) and calculated structural formulae for feldspars in the Foeni ceramics.

Sample/micropoint	CE-80-1-2	CE-80-1-13	CE-80-3-11	CE-80-4-4	CE-80-4-5	CE-83-1-1	CE-83-1-2	CE-83-1-7	CE-83-3-11	CE-83-3-6	CE-83-3-8	CE-83-1-11	CE-83-1-3	CE-83-1-5	CE-83-3-12	CE-83-3-5
	Afs	Afs	Afs	Afs	Afs	Afs	Afs	Afs	Afs	Afs	Pl	Pl	Pl	Pl	Pl	Pl
SiO <sub>2</sub>	65.10	63.64	64.95	63.32	63.56	62.68	63.59	63.28	65.41	64.01	62.34	62.27	57.95	59.10	63.74	66.00
Al <sub>2</sub> O <sub>3</sub>	18.10	17.95	18.07	17.82	17.95	17.80	17.70	17.92	17.57	17.89	22.34	21.95	24.01	23.23	21.34	20.28
TiO <sub>2</sub>	bdl	bdl	bdl	bdl	bdl	0.06	bdl	0.06	bdl	bdl	bdl	bdl	bdl	bdl	bdl	bdl
FeO	0.13	0.07	0.10	0.18	0.11	0.19	0.17	0.09	0.10	0.13	0.12	0.07	0.15	0.11	0.08	0.07
BaO	0.07	0.15	0.08	0.48	0.28	0.75	0.30	0.68	bdl	0.36	bdl	bdl	bdl	bdl	bdl	bdl
CaO	bdl	bdl	bdl	bdl	bdl	0.03	bdl	bdl	0.12	bdl	4.27	3.84	6.64	5.63	3.23	1.65
Na <sub>2</sub> O	0.79	0.85	0.45	0.31	0.34	0.27	0.35	0.54	0.04	0.13	9.16	9.47	7.70	8.44	9.71	11.05
K <sub>2</sub> O	16.13	16.12	16.65	16.74	16.56	15.27	16.13	16.37	13.96	16.78	0.11	0.09	0.10	0.07	0.26	0.07
Total	100.32	98.78	100.30	98.88	98.81	97.05	98.25	98.94	97.20	99.30	98.34	97.69	96.55	96.58	98.36	99.12
Si	6.01	5.98	6.01	5.98	5.98	6.00	6.01	5.97	6.12	6.00	5.61	5.64	5.36	5.45	5.72	5.85
Al	1.97	1.99	1.97	1.98	1.99	2.00	1.97	1.99	1.94	1.97	2.37	2.34	2.61	2.52	2.26	2.12
Fe <sup>2+</sup>	0.01	0.01	0.01	0.01	0.01	0.02	0.01	0.01	0.01	0.01	0.01	0.01	0.01	0.01	0.01	0.01
Ca	0	0	0	0	0	0	0	0	0.01	0	0.41	0.37	0.66	0.56	0.31	0.16
Na	0.14	0.16	0.08	0.06	0.06	0.05	0.06	0.10	0.01	0.02	1.60	1.66	1.38	1.51	1.69	1.90
K	1.90	1.93	1.96	2.02	1.99	1.86	1.94	1.97	1.67	2.01	0.01	0.01	0.01	0.01	0.03	0.01
Total cations	10.03	10.06	10.03	10.06	10.04	9.95	10.01	10.06	9.75	10.03	10.01	10.03	10.03	10.05	10.01	10.04
An	0	0	0	0	0	0.2	0	0	0.7	0	20.4	18.2	32.1	26.8	15.3	7.6
Ab	6.9	7.4	4	2.7	3	2.6	3.2	4.8	0.4	1.2	79	81.3	67.3	72.8	83.2	92
Or	93.1	92.6	96	97.3	96.9	97.2	96.8	95.2	98.9	98.8	0.6	0.5	0.6	0.4	1.5	0.4

Fe<sub>TOT</sub> as FeO.Calculations on an 8 O basis, according to Deer *et al.* (1992).

Afs = alkali feldspar; bdl = below detection limit; Pl = plagioclase.

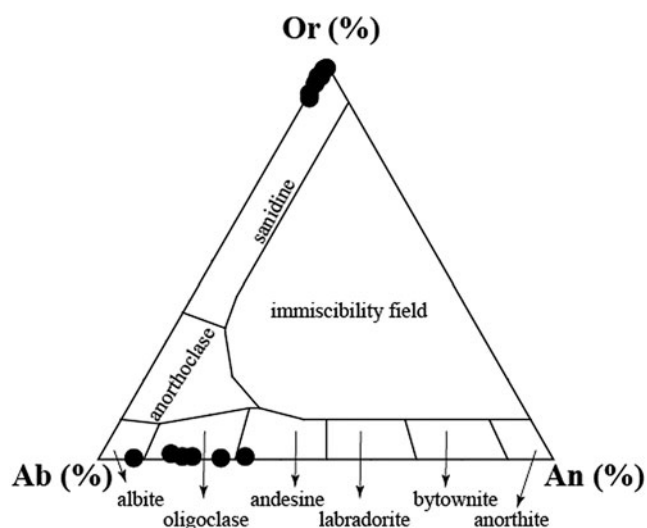


**Fig. 8.** Chemistry of feldspars in the Foeni sherds: plot of EMPA data in the feldspar classification diagram.

Parts of the Foeni sherds show reddish hues and contain hematite (Fig. 4). Generally, a reddish colour for ceramics is obtained when clays rich in iron oxides are used for the paste (Molera *et al.*, 1998; De Bonis *et al.*, 2017). No spinel lines were identified in the XRD traces of the dark grey sherds, possibly because of the small size and the small amount of spinel grains.

The EMPA data revealed a relatively large amount of  $P_2O_5$  in the matrix (Table 3, Fig. 7c). The CaO vs.  $P_2O_5$  diagram (Fig. 7c) displays two groups of data, one with higher calcium and phosphorous contents (A) and another with lower calcium and phosphorous contents (B). The nature of crystalloclasts and pedogenic

concretions as well as the positive correlation ( $\sim 0.8$ ) between  $P_2O_5$  and CaO for group A indicate apatite as the source of P for part of the matrix (see also Ionescu *et al.*, 2011; Ionescu & Hoeck, 2017). Alternatively, phosphorous may be due to burial (Freestone *et al.*, 1985, 1994; Maritan & Mazzoli, 2004; Maritan *et al.*, 2009) in the case of the group B data.

Miocene illitic clays containing small amounts of montmorillonite cropping out towards the northeast of the cave were used for a younger pottery, namely Coțofeni (also from the Copper Age), found in the same cave (Giurgiu *et al.*, 2017). The use of the same raw material for the Coțofeni and Foeni pottery is supported by the X-ray elemental mapping (Fig. 9) and by the EMPA microchemical data for the clay minerals in the matrix of the Foeni ceramics. The latter shows the presence of a small amount of Ca. The overall composition of the Foeni matrix matches that of the matrix of the Coțofeni sherds (Fig. 10a,b). It is highly plausible that the same raw illitic material, with a minor montmorillonite content, was used by both the Foeni and the Coțofeni people. As long as the raw materials had the characteristics required to provide high-quality ceramics, people would use such known sources.

The hiatal distribution of the grain size, at least for the coarser sherds, demonstrates the use of a small amount of artificial temper, added by the potter to better control plasticity (Maggetti, 1979). The composition of the clasts, with quartz, feldspars, muscovite, biotite and chlorite, the heavy minerals and the rock fragments (quartzite, micaschist and amphibolitic schist) fit the mineralogical and petrographic nature of the Cerna River catchment area in the Southern Carpathians (Fig. 1). Granodiorites and gneisses are sources of quartz, feldspars and some heavy minerals, such as amphibole, epidote and apatite. The composition of plagioclase in our samples is typical of greenschist-amphibolite metamorphic facies and is common in the area. Garnets, muscovite and biotite also originate from gneisses. Mica schists provide phengitic

**Table 5.** Selected EMPAs (mass%) for muscovite in the Foeni ceramics.

Sample/micropoint	CE-80-1-1	CE-80-1-10	CE-80-1-15	CE-80-1-3	CE-80-1-5	CE-80-1-7	CE-80-2-12
SiO <sub>2</sub>	48.05	49.47	50.84	46.91	49.51	52.34	49.33
Al <sub>2</sub> O <sub>3</sub>	31.62	29.38	26.87	31.30	29.83	26.86	27.07
TiO <sub>2</sub>	0.19	0.41	0.11	0.32	0.11	0.58	0.44
FeO	3.86	2.10	1.92	4.10	1.64	3.56	5.13
MnO	bdl	bdl	0.03	bdl	bdl	bdl	bdl
MgO	0.93	2.31	3.77	0.90	2.29	3.48	2.28
BaO	0.17	0.69	0.89	0.21	0.12	0.17	0.17
CaO	0.02	0.02	0.21	bdl	bdl	0.07	0.84
Na <sub>2</sub> O	0.75	0.30	0.19	0.54	0.20	0.15	0.32
K <sub>2</sub> O	6.29	6.93	7.19	4.08	6.34	8.90	6.49
Total	91.71	90.93	91.14	88.16	89.93	96.03	91.91
Si	6.54	6.73	6.91	6.55	6.76	6.88	6.77
Al <sup>IV</sup>	1.46	1.27	1.09	1.45	1.24	1.12	1.23
Sum T	8	8	8	8	8	8	8
Al <sup>VI</sup>	3.60	3.44	3.20	3.69	3.56	3.04	3.15
Ti	0.02	0.04	0.01	0.03	0.01	0.06	0.05
Fe <sup>2+</sup>	0.44	0.24	0.22	0.48	0.19	0.39	0.59
Mn	0	0	0	0	0	0	0
Mg	0.19	0.47	0.76	0.19	0.47	0.68	0.47
Ca	0	0	0.03	0	0	0	0.12
Na	0.20	0.08	0.10	0.15	0.05	0.04	0.10
K	1.09	1.20	1.25	0.73	1.11	1.49	1.14
Total cations	13.54	13.47	13.53	13.26	13.39	13.73	13.59
Fe/(Fe + Mg)	0.70	0.34	0.22	0.72	0.29	0.36	0.56
Mg/(Fe + Mg)	0.30	0.66	0.78	0.28	0.71	0.64	0.44

Fe<sub>TOT</sub> as FeO.

Calculated structural formulae for muscovite on a 22 O basis, according to Deer *et al.* (1992).

bdl = below detection limit; Sum T = total cations in tetrahedral sites.

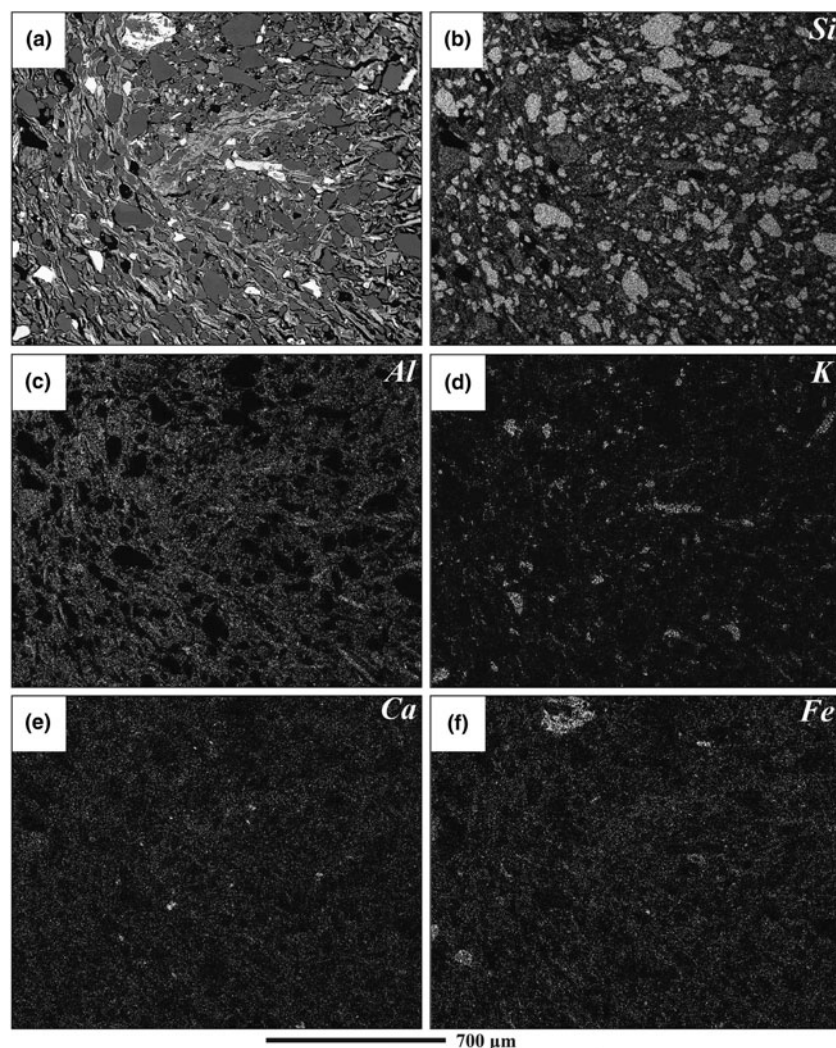


**Fig. 9.** X-ray compositional maps of sample CE-83. (a) BSE image showing grains of quartz (dark grey), plagioclase (grey) and alkali feldspar (light grey) in a matrix consisting of an illite-like mineral and muscovite (speckled grey). (b) Distribution of Si in quartz and silicates. (c) Distribution of Al in aluminosilicates. (d) Distribution of K in the illitic matrix, muscovite and alkali feldspars. (e) Homogeneous distribution of Ca in the matrix. (f) Homogeneous distribution of Fe in the matrix. The black areas are pores. The brightness of dots for the K, Ca and Fe distributions is enhanced in order to give a clearer view. The same scale is used for all images.

muscovite and biotite, whereas chlorite schists are the main sources of chlorite. The iron pellets and graphite lamellae are linked to the iron ore and the graphitic schist, respectively, cropping out west of Teliuc (Fig. 1). The lack of crystalline dolomite clasts in the Foeni sherds indicates production far away from areas where such rocks crop out (*i.e.* in the host rock of the GCC).

The scarcity of chamotte fragments demonstrates that this kind of artificial temper was not commonly used, in contrast to the later Copper Age pottery discovered in the same cave (Giurgiu *et al.*, 2017). The presence of the clay pellets is due to an insufficiently homogenized ceramic paste (Medeghini & Nigro, 2017) or to unseasoned clay (Maritan, 2004).

The Foeni potters mixed Fe-rich, poorly carbonatic illitic clay with alluvial sand to model various vessels by hand. The workshops were not emplaced at the cave, which was used only as a temporary shelter, but probably further to the east, somewhere close to the Cerna River, where clays, sands and water were at hand (Fig. 1).

#### Firing constraints

The homogeneous bodies of four of the sherds suggest constant redox conditions of a firing atmosphere. The four sherds displaying reddish–brown colours (Table 1) and containing larger amounts of hematite (Fig. 4) were fired in an oxidizing atmosphere (Shepard,

1976; Murad & Wagner, 1996; Molera *et al.*, 1998), whereas the dark grey sherd is due to firing in a constant but reducing atmosphere. For the three black-topped samples, the firing conditions were different. Firing experiments carried out in open air or in kilns by Davies (1962), Hendrickx *et al.* (2000), Baba & Saito (2004), Bințințan (2013) and Bințințan & Gligor (2016) demonstrated that this type of pottery may be obtained by arranging the vessels bottom-up on a floor covered by chaff, sawdust, oak wood or a mix of carbon and ash. The firing temperature should not exceed 950°C (Dufournier, 1986).

The thermal constraints for the pottery are provided by OM, XRPD and EMPA data. The optical characteristics of the matrix reflect the changes in the clay minerals' crystalline structure upon firing (Maggetti, 1982). Most of the Foeni sherds show a highly birefringent matrix, consisting of clay minerals and micas sintered together. The crystal structure of the clay minerals and muscovite is only slightly affected by temperature. In the few sherds with a low-birefringent matrix and in between isotropic areas, the crystalline structure collapsed partially and the material became amorphous. Yet the temperature was not high enough to melt the material and obtain glass.

The intensity and width of the diffraction peaks also offer details about the crystalline state of clay minerals and muscovite. The illite-muscovite XRPD peaks are still present in the material fired

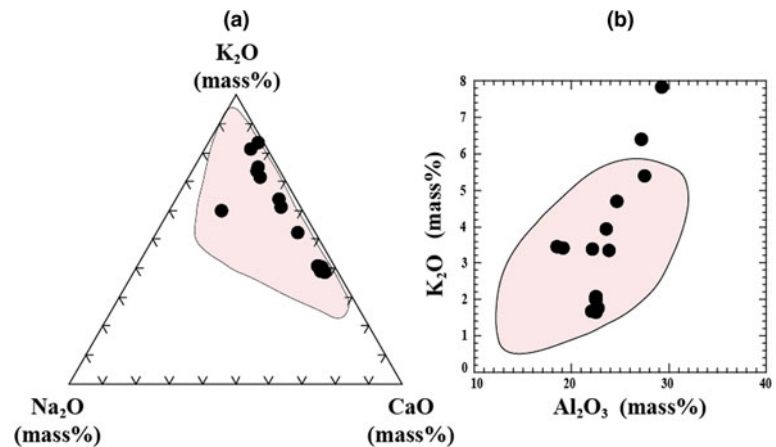


**Fig. 10.** Comparison of the EMPA data obtained for the ceramic matrix of the Copper Age Foeni (this study) and Coțofeni sherds (data from Giurgiu *et al.*, 2017). (a) K<sub>2</sub>O vs. Na<sub>2</sub>O vs. CaO diagram. (b) K<sub>2</sub>O vs. Al<sub>2</sub>O<sub>3</sub> diagram. Black dots = Foeni sherds, shaded areas = fields of the Coțofeni sample plots.

at 800°C (Mercader *et al.*, 2000). Illite begins to decompose at 820°C (Heimann, 2017). The diminishing of the illite-muscovite diffraction peaks indicates a partial destruction of the crystalline structure and suggests firing probably at ~850°C (Broekmans *et al.*, 2004; Ionescu *et al.*, 2007). At temperatures >900°C, the peaks of clay minerals are absent (DeVito *et al.*, 2014). The illite-muscovite diffraction peaks for most of the Foeni samples are intense and sharp (Fig. 4), marking a crystalline structure and a temperature at ~800°C. The sherds CE-77 and CE-79 show a diminished 1 nm peak, which is consistent with firing at ~850°C. There are no X-ray traces lacking the illite-muscovite peaks, thus pointing to firing temperatures of <900°C for all samples. The intensity of the feldspar peaks (in particular the 0.32 nm peak) reflects different amounts of feldspar in the raw material rather than feldspar formation upon firing. The lower K<sub>2</sub>O values recorded in the matrix material from Foeni are due to the dehydroxylation of illite (Guggenheim *et al.*, 1987; Rosenberg, 2002; Rodriguez-Navarro *et al.*, 2003; Gualtieri & Ferrari, 2006). The increasing CaO content is attributed to its incorporation upon firing at ~850°C (Ionescu & Hoeck, 2011).

Consequently, the results are corroborated by the lack of specific firing phases such as spinel or pyroxene, suggesting that the Foeni sherds were fired at a temperature of <850°C (see also Murad & Wagner, 1996; Ionescu *et al.*, 2007), which is within the normal range recorded in bonfires and surface clamps (Velde & Druc, 1999). The temperature range was high enough to obtain a sintered ceramic body, holding together clay minerals, micas and various aplastic fragments. However, a homogeneous temperature is difficult to acquire (*cf.* Gosselain, 1992; Thér, 2004, 2014) and differences of up to 250°C were measured in experimental clamp-kilns by Thér (2004). Moreover, inside the same pot, the thermal differences may reach several hundreds of degrees centigrade (Magetti *et al.*, 2011). Considering the relatively narrow temperature interval of 50°C estimated for the Foeni sherds, it is probable that the pottery was fired in similar conditions (*i.e.* in bonfires). The experimental production of black-topped ceramics (Hendrickx *et al.*, 2000; Baba & Saito, 2004; Bințișan, 2013; Bințișan & Gligor, 2016) suggests that the primitive firing structures were temporary (used for one or a few loads) and were reconstructed seasonally.

## Conclusions

The compositional and microstructural characteristics of the sherds helped to unveil the type and origin of the raw materials as well as the technological level of the potters. Despite the

primitive firing conditions in bonfires or surface clamps and the relatively low temperature attained, the potters produced blacked-topped ceramics, showing care for the aesthetical aspects and a certain control of the atmosphere in the kiln. The same raw materials were probably quarried and used at different times by different people. For example, later in the Copper Age, the Coțofeni people processed essentially the same raw materials as the Foeni people, suggesting a continuity of knowledge and tradition in producing ceramic wares.

**Acknowledgements.** The study was financed by the Excellence Research Program (Romanian Ministry of Education and Ministry of Research) through the UEFISCDI/CNCS project PN-III-P4-ID-PCE-2016-0229 (awarded to C.I.). Dr Sorin Tincu from the Corvin Castle Museum is gratefully acknowledged for providing the sherds. C.I. also acknowledges the support within the Program of competitive growth of Kazan Federal University, awarded by the Russian Government. Comments by two anonymous reviewers significantly helped to improve the manuscript.

## References

- Baba M. & Saito M. (2004) Experimental studies on the firing methods of black topped pottery in Predynastic Egypt. Pp. 575–589 in: *Egypt at Its Origins: Studies in Memory of Barbara Adams: Proceedings of the International Conference, 'Origin of the State: Predynastic and Early Dynastic Egypt', Kraków, 28th August–1st September 2002* (S. Hendrickx, R.F. Friedman, K.M. Ciałowicz & M. Chłodnicki, editors). Orientalia Lovaniensia Analecta 138. Peeters Publishing, Leuven, Belgium.
- Balintoni I. (1997) *Geotectonics of the Metamorphic Terrains from Romania*. Ed. Carpatica, Cluj-Napoca, Romania, 176 pp. (in Romanian).
- Balintoni I., Balica C., Ducea M.N. & Hann H.P. (2014) Peri-Gondwanan terranes in the Romanian Carpathians: a review of their spatial distribution, origin, provenance, and evolution. *Geoscience Frontiers*, 5, 395–411.
- Balintoni I., Balica C., Ducea M.N., Chen F., Hann H.P. & Șabliovschi V. (2009) Late Cambrian–early Ordovician Gondwanan terranes in the Romanian Carpathians: a zircon U–Pb provenance study. *Gondwana Research*, 16, 119–133.
- Bințișan A. (2013) Experimental archaeology. Controlled firing in open air – a possible way for obtaining blacked-topped chromatic effect. *Buletinul Cercurilor Științifice Studentești*, 19, 7–19 (in Romanian).
- Bințișan A. & Gligor M. (2016) Pottery kiln: a technological approach to early Eneolithic black-topped production in Transylvania. *Studia Antiqua et Archaeologica*, 22, 5–18.
- Bințișan A., Gligor M., Dulamă I.D., Rădulescu C., Stihî C., Ion R.M., Teodorescu S., Știrbescu R.M., Bucurică I.A. & Pehoiu G. (2019) Analysis and structural investigations on early Eneolithic Foeni painted pottery from Alba Iulia–Lumea Noua archaeological site. *Romanian Journal of Physics*, 64, 903.

- Broekmans T., Adriaens A. & Pantos E. (2004) Analytical investigations of cooking pottery from Tell Beydar (NE-Syria). *Nuclear Instruments and Methods in Physics Research B*, **226**, 92–97.
- Carroll D. (1970) Clay minerals: a guide to their X-ray identification. *Geological Society of America Special Papers*, **126**, 1–80.
- Davies P. (1962) Red and black Egyptian pottery. *Journal of Egyptian Archaeology*, **48**, 19–24.
- De Bonis A., Cultrone G., Grifa C., Langella A., Leone A.P., Mercurio M. & Morra V. (2017) Different shades of red: the complexity of mineralogical and physicochemical factors influencing the colour of ceramics. *Ceramics International*, **43**, 8065–8074.
- Deer W.A., Howie R.A. & Zussman J. (1992) *An Introduction to the Rock-Forming Minerals*, 2nd edn. Pearson Prentice Hall, London, UK, 696 pp.
- DeVito C., Medeghini L., Mignardi S., Orlandi D., Nigro L., Spagnoli F., Lottici P.P. & Bersani D. (2014) Technological fingerprints of Black-Gloss Ware from Motya (Western Sicily, Italy). *Applied Clay Science*, **88–89**, 202–213.
- Draşovean F. (1994) The Petreşti culture in Banat. *Studies on the History of Banat*, **XVI**, 1–45 (in Romanian).
- Draşovean F. (2013) About some synchronisms from the late Neolithic and Early Eneolithic in Banat and Transylvania. A Bayesian approach of some absolute data previously published. *Analele Banatului, Arheologie–Istorie*, **XXI**, 11–34 (in Romanian).
- Dufournier D. (1986) Analyse de la céramique, premiers résultats. Pp. 444–446 in: *Saï 1 La nécropole Kerma* (B. Gratien, editor). Editions du CNRS, Paris, France.
- Fabbri B., Gligor M., Gualtieri S. & Varvara S. (2009) Archaeometric comparison between the Neolithic pottery of different cultures at the archaeological site of Alba Iulia (Transylvania, Romania). *Studia Universitatis Babeş-Bolyai Geologia*, **54**, 23–26.
- Fabbri B., Gualtieri S., Varvara S. & Gligor M. (2008) Archaeometric characterisation of Foeni pottery from the Alba Iulia–Lumea Nouă archaeological site (Romania). Pp. 128–139 in: *Absolute Ages Obtained by Radiometric Dating* (C. Cosma, S. Varvara & M. Gligor, editors). Quantum, Cluj-Napoca, Romania (in Romanian).
- Freestone I.C., Meeks N.D. & Middleton A.P. (1985) Retention of phosphate in buried ceramics: an electron microbeam approach. *Archaeometry*, **27**(2), 161–177.
- Freestone I.C., Middleton A.P. & Meeks N.D. (1994) Significance of phosphate in ceramic bodies: discussion of paper by Bollong et al. *Journal of Archaeological Science*, **21**, 425–426.
- Gál Á., Ionescu C., Bajusz M., Codrea V.A., Hoeck V., Barbu-Tudoran L., Simon V., Mureşan-Pop M. & Csók Z. (2018) Composition, technology and provenance of Roman pottery from Napoca (Cluj-Napoca, Romania). *Clay Minerals*, **53**, 621–641.
- Gherasi N., Mureşan M., Mureşan G., Krätner H., Krätner F., Lupu M., Marinescu F., Savu H. & Drăgulescu A.A. (1967) *Geological Map of Romania, 1:200,000, Deva File*. Geological Institute of Romania, Bucharest, Romania.
- Giurgiu A., Ionescu C., Šarić K., Tămaş T., Roman C. & Crandell O. (2015) SEM study of surface decorations of Neolithic–Chalcolithic ceramic pots from the Cerişor Cave (Southern Carpathians, Romania). Presented at: *14th European Meeting on Ancient Ceramics*, Athens, Greece.
- Giurgiu A., Ionescu C., Hoeck V., Tămaş T., Roman C. & Crandell O. (2017) Insights into the raw materials and technology used to produce Copper Age ceramics in the Southern Carpathians (Romania). *Archaeological and Anthropological Sciences*, **9**, 1259–1273.
- Gligor M. (2007a) Preventive archaeological research at Alba Iulia–Lumea Nouă. A discovery of material belonging to the Foeni Group. *Apulum*, **XLIV**, 1–28 (in Romanian).
- Gligor M. (2007b) Foeni cultural group. Pp. 51–63 in: *A History Lesson – Pottery Manufacturing 8000 Years Ago* (B. Ciută, C. Florescu, M. Gligor, P. Mazăre, C. Şeteu & S. Varvara, editors). Aeternitas Publishing, Alba Iulia, Romania.
- Gligor M. (2008a) Contributions to the catalogue of discoveries of the Foeni Group in Romania. *Patrimonium Apulense*, **7–8**, 11–18 (in Romanian).
- Gligor M. (2008b) On the Neolithic settlement from Petreşti-Groapa Galbenă. *Apulum*, **XLV**, 293–314 (in Romanian).
- Gligor M. (2009a) Foeni ceramic materials from Transylvania. *Annales Universitatis Apulensis, Series Historica*, **13**, 51–55 (in Romanian).
- Gligor M. (2009b) *The Neolithic and Eneolithic Settlement from Alba Iulia–Lumea Nouă in the Focus of Recent Research*. Ed. Mega, Cluj-Napoca, Romania, 487 pp. (in Romanian).
- Gligor M. (2014) The beginnings of the early Eneolithic in Transylvania: a Bayesian approach. *Analele Banatului*, **XXII**, 91–105 (in Romanian).
- Gosselain O.P. (1992) Bonfire in the enquiries. Pottery firing temperatures in archaeology: what for? *Journal of Archaeological Sciences*, **19**, 243–259.
- Gualtieri A.F. & Ferrari S. (2006) Kinetics of illite dehydroxylation. *Physics and Chemistry of Minerals*, **33**, 490–501.
- Guggenheim S., Chang Y.H. & van Gross K.A.F. (1987) Muscovite dehydroxylation: high-temperature studies. *American Mineralogist*, **72**, 537–550.
- Heimann R. (2017) X-ray powder diffraction (XRPD). Pp. 327–341 in: *The Oxford Handbook of Archaeological Ceramic Analysis* (A.M.W. Hunt, editor). Oxford University Press, Oxford, UK.
- Heinrich K.F.J. (1991) Strategies of electron probe data reduction. Pp. 9–18 in: *Electron Probe Quantitation* (K.F.J. Heinrich & D.E. Newbury, editors). Plenum Press, New York, NY, USA.
- Hendrickx S., Friedman R. & Loyens F. (2000) Experimental archaeology concerning black-topped pottery from Ancient Egypt and the Sudan. *Cahiers de la Céramique Égyptienne*, **6**, 171–187.
- Ionescu C., Ghergari V., Horga M. & Rădulescu G. (2007) Early Medieval ceramics from the Viile Tecii archaeological site (Romania): an optical and XRD study. *Studia Universitatis Babeş-Bolyai Geologia*, **52**, 29–35.
- Ionescu C. & Hoeck V. (2011) Firing-induced transformations in Copper Age ceramics from NE Romania. *European Journal of Mineralogy*, **23**, 937–958.
- Ionescu C., Hoeck V., Crandell O.N. & Šarić K. (2015) Burnishing versus smoothing in ceramic surface finishing: a SEM study. *Archaeometry*, **57**, 18–26.
- Ionescu C., Hoeck V. & Ghergari L. (2011) Electron microprobe analysis of ancient ceramics: a case study from Romania. *Applied Clay Science*, **53**, 466–475.
- Ionescu C. & Hoeck V. (2017) Electron microprobe analysis (EMPA). Pp. 288–304 in: *The Oxford Handbook for Archeological Ceramic Analysis* (A.M.V. Hunt, editor), Oxford University Press, Oxford, UK.
- Krätner H.G. (1977) Hydrothermal–sedimentary iron ores related to submarine volcanic rises: the Teliuc–Ghelar type as a carbonatic equivalent of the Lahn–Dill type. Pp. 232–253 in: *Time- and Strata-Bound Ore Deposits* (D.D. Klemm & H.J. Schneider, editors). Springer, Berlin, Germany.
- Luca S.A., Roman C. & Diaconescu D. (2004) *Archaeological Research in Cauca Cave (Vol. 1)*. Ed. Economică, Bucharest, Romania, 288 pp. (in Romanian).
- Maggetti M. (1979) Mineralogisch-petrographische Untersuchung des Scherbenmaterials der urnenfelderzeitlichen Siedlung Elchinger Kreuz, Ldkr. Neu-Ulm/Donau. *Kataloge Prähistorische Staatssammlung München*, **19**, 141–172.
- Maggetti M. (1982) Phase analysis and its significance for technology and origin. Pp. 121–133 in: *Archaeological Ceramics* (J.S. Olin & A.D. Franklin, editors). Smithsonian Institution Press, Washington, DC, USA.
- Maggetti M., Neururer C. & Ramseyer D. (2011) Temperature evolution inside a pot during experimental surface (bonfire) firing. *Applied Clay Science*, **53**, 500–508.
- Maritan L. (2004) Archaeometric study of Etruscan–Padan type pottery from the Veneto region: petrographic, mineralogical and geochemical-physical characterization. *European Journal of Mineralogy*, **16**, 297–307.
- Maritan L., Angelini I., Artioli G., Mazzoli C. & Saracino M. (2009) Secondary phosphates in the ceramic materials from Frattesina (Rovigo, north-eastern Italy). *Journal of Cultural Heritage*, **10**, 144–151.
- Maritan L. & Mazzoli C. (2004) Phosphates in archaeological finds: implications for environmental conditions of burial. *Archaeometry*, **46**, 673–683.
- Medeghini L. & Nigro L. (2017) Khirbet al-Batrawy ceramics: a systematic mineralogical and petrographic study for investigating the material culture. *Periodico di Mineralogia*, **86**, 19–35.
- Mercader J., Garcia-Heras M. & Gonzalez-Alvarez I. (2000) Ceramic tradition in the African forest: characterisation analysis of ancient and modern pottery from Ituri, D.R. Congo. *Journal of Archaeological Science*, **27**, 163–182.
- Molera J., Pradell T. & Vendrell-Saz M. (1998) The colours of Ca-rich ceramic pastes: origin and characterization. *Applied Clay Science*, **13**, 187–202.

- Moore D.M. & Reynolds Jr. R.C. (1997) *X-Ray Diffraction and the Identification and Analysis of Clay Minerals*. Oxford University Press, Oxford, UK, 378 pp.
- Munsell A. (1994) *Munsell Soil Colour Charts*. Munsell Colour, New Windsor, NY, USA, 10 pp.
- Murad E. & Wagner U. (1996) The thermal behavior of an Fe-rich illite. *Clay Minerals*, **31**, 45–52.
- Mureșan M., Mureșan G. & Krätner H.G. (1980) *Geological Map of Romania, 1:50,000, Hunedoara Sheet*. Geological and Geophysical Institute of Romania, Bucharest, Romania.
- Rodriguez-Navarro A., Cultrone G., Sanchez-Navas A. & Sebastian E. (2003) TEM study of mullite growth after muscovite breakdown. *American Mineralogist*, **88**, 713–724.
- Roman C., Diaconescu D. & Luca S.A. (2000) Archaeological research in Cerișor Cave No. 1 (Great Cave) (Leleșe village, Hunedoara County). *Acta Musei Corvinensis*, **6**, 7–59 (in Romanian).
- Rosenberg P.E. (2002) The nature, formation, and stability of end-member illite: a hypothesis. *American Mineralogist*, **87**, 103–107.
- Shepard A.O. (1976) *Ceramics for the Archaeologist*. Carnegie Institute, Washington, DC, USA, 414 pp.
- Spataro M. (2011) A comparison of chemical and petrographic analyses of Neolithic pottery from south-eastern Europe. *Journal of Archaeological Science*, **38**, 255–269.
- Taylor B.N. (2001) *The International System of Units (SI)*. US National Institute of Standards and Technology Special Publication 330. National Institute of Standards and Technology, Washington, DC, USA, 75 pp.
- Thér R. (2004) Experimental pottery firing in closed firing devices from the Neolithic–Hallstatt period in Central Europe. *EuroREA*, **1**, 35–82.
- Thér R. (2014) Identification of pottery firing structures using the thermal characteristics of firing. *Archaeometry*, **56**, 78–99.
- Velde B. & Druc C.I. (1999) *Archaeological Ceramic Materials. Origin and Utilization*. Springer, Berlin, Germany, 299 pp.
- Wentworth C.K. (1922) A scale of grade and class terms for clastic sediments. *Journal of Geology*, **30**, 377–392.
- Whitney D.L. & Evans B.W. (2010) Abbreviations for names of rock forming minerals. *American Mineralogist*, **95**, 185–187.